AIAA JOURNAL
Vol. 44, No. 7, July 2006

Role of $O_2(b)$ and I_2 (A', A) in Chemical Oxygen–Iodine Laser Dissociation Process

Valeriy N. Azyazov* and Michael C. Heaven†
Emory University, Atlanta, Georgia 30322

Kinetic studies were carried out to explore the role of electronically excited iodine [$I_2(A', A)$] in the dissociation of I_2 by singlet oxygen, and the possible role of $I_2 + O_2(b)$ energy transfer as the initiation step of the dissociation sequence. Flow-tube measurements that utilized a chemical singlet oxygen generator were used evaluate the contribution of the $O_2(b) + I_2$ reaction. The rate of I_2 dissociation was examined under conditions where varying concentrations of CO_2 were used to quench $O_2(b)$. Pulsed laser pump-probe experiments were used to study the relaxation kinetics of $I_2(A')$. Rate constant for quenching of $I_2(A')$ by Ar (2.7×10^{-14} cm^3/s), I_2 (4.8×10^{-11} cm^3/s), and CO_2 (8.5×10^{-13} cm^3/s) were measured. An I_2 dissociation model in which the electronically excited intermediate $I_2(A'$ or $A)$ is populated by collisions with vibrationally excited $O_2(a)$ was found to be in good agreement with experiment.

Nomenclature

A_{1268}	=	Einstein coefficient for the $O_2a \rightarrow X$ transition
A_{1315}	=	Einstein coefficient for the $I^* \rightarrow I$ transition
C	=	detectivity correction coefficient
D	=	diffusion coefficient
d_{mix}	=	mixing scale transverse to the gas flow
G^p_{buf}, G^s_{buf}	=	flow rates of primary and secondary buffer gases
G_{Cl_2}, G_{I_2}	=	flow rates of gaseous chlorine and iodine
G_i	=	flow rate of ith component
H, B	=	height and width of the gas duct of the measuring cell
I, I^*	=	atomic iodine in the electronic states $^2P_{3/2}$ and $^2P_{1/2}$
I_{B-X}	=	intensity of the $I_2B \rightarrow X$ emission band
I_{Ge}	=	signal from a Ge photodetector
$I_2^\dagger$	=	vibrationally excited $I_2(X)$ in levels above $v = 20$
$I_2(X)$, $I_2(A')$, $I_2(A)$, $I_2(B)$	=	iodine molecule in the electronic states $X^1\Sigma_g^+$, $A'^3\Pi_{2u}$, $A^3\Pi_{1u}$, $B^3\Pi_{0_u^+}$
K_i	=	rate constant coefficient of ith reaction
$K_{v',v''}$	=	rate constant coefficient for vibrational-vibrational exchange process
L	=	downstream distance along the flow cell
l_{mix}	=	length of mixing zone along the flow
N_a, N_b	=	concentrations of $O_2(a)$ and $O_2(b)$
N_{I^*}	=	concentration of electronically excited atomic iodine
N_{I_2}, N_w	=	vapor concentrations of I_2 and H_2O
N_{O_2}	=	concentration of oxygen molecules in all electronic states
$O_2(X)$, $O_2(a)$, $O_2(b)$	=	oxygen molecule in the electronic states $X^3\Sigma_g^-$, $a^1\Delta_g$, $b^1\Sigma_g^+$
P_{buf}	=	partial pressure of buffer gas
P_{CO_2}, P_{I_2}	=	partial pressures of CO_2 and I_2
P_c	=	gas pressure in measuring cell
T	=	gas temperature
U	=	gas velocity
v	=	vibrational quantum number
$\gamma_{i,j}$	=	excitation probability of the jth vibrational level in ith energy transfer process
η_{I_2}, η_w	=	relative densities of iodine and water vapor
η_i	=	relative density of ith component

Presented as Paper 2005-5037 at the AIAA 36th Plasmadynamics and Lasers Conference, Toronto, ON, Canada, 6–9 June 2005; received 15 June 2005; revision received 8 November 2005; accepted for publication 22 November 2005.

*Visiting Scientist, Department of Chemistry; azyazov@fian.smr.ru.
†Professor, Department of Chemistry; heaven@euch4e.emory.edu. Member AIAA.

I. Introduction

THE mechanism by which singlet oxygen dissociates I_2 in the chemical oxygen–iodine laser (COIL) remains as an important unsolved problem. The dissociation efficiency can be described empirically in terms of the number of singlet oxygen molecules $O_2(a)$ needed to dissociate one I_2 molecule. As the dissociation process involves several steps, this is not fixed number, but an effective parameter that depends on the local conditions at the point of I_2 injection and the fluid dynamics subsequent to injection. The impact of the dissociation energy cost on the chemical efficiency of the laser was recently highlighted by the work Rybalkin et al.[1] They reported that the efficiency of their laser increased from 33 to 40% when the mode of I_2 injection was modified. The enhanced performance was attributed to improvement in the dissociation efficiency.

The standard COIL kinetics model assumes that dissociation occurs via the sequence

$$O_2(a) + I_2(X) \rightarrow O_2(X) + I_2^\dagger \tag{32}$$

$$O_2(a) + I_2^\dagger \rightarrow O_2(X) + 2I \tag{34}$$

where $I_2^\dagger$ is $I_2(X)$ in vibrationally excited levels above $v = 20$. (The equation numbering used here is that of the standard kinetic package.[2]) Once initiated, the dissociation process is accelerated by the chain branching steps

$$O_2(a) + I \rightarrow O_2(X) + I^* \tag{40}$$

$$I^* + I_2(X) \rightarrow I_2^\dagger + I \tag{33}$$

Recent experimental studies have raised doubts concerning this mechanism. It has been shown that the relaxation kinetics for $I_2^\dagger$ are not in agreement with the deactivation kinetics for the excited intermediate of the COIL model.[3] Overall, the dependence of the $I_2^\dagger$ deactivation rate constant on the identity of the collision partner is more consistent with the quenching of an electronically excited

intermediate.[4,5] Furthermore, direct measurement of the rate constant for quenching of $O_2(a)$ by $I_2(X)$ yields an upper bound for the rate constant for reaction (32) that is at least an order of magnitude smaller than the value required by the model.[6]

Derwent and Thrush[7] and Derwent et al.[8] proposed a model for the dissociation process where $I_2(X)$ was dissociated by energy transfer from $O_2(b)$:

$$O_2(b) + I_2(X) \rightarrow O_2(X) + 2I \tag{21}$$

Kinetic simulations based on this reaction were successful in reproducing the results from flow-tube kinetics experiments, but this model was abandoned when measurements of the $O_2(b) + I_2(X)$ quenching rate constant indicated that the reaction was not fast enough to account for the observed I_2 dissociation rates.[9,10] When the problem with reaction (32) was discovered, Heaven et al.[11] remeasured the rate constant for reaction (21). They found that K_{21} was larger than the earlier estimates (3×10^{-11} vs 4×10^{-12} cm^3/s), but still not large enough to rescue the Derwent and Thrush[7] and Derwent et al.[8] model. However, the larger rate constant suggested the possibility that reaction (21) might be fast enough to replace reaction (32) as the initiator of the dissociation sequence.

Arnold et al.[12] considered the possibility that electronically excited states of I_2 are involved in the dissociation process via the sequence

$$O_2(a) + I_2(X) \rightarrow O_2(X) + I_2(A', A) \tag{19}$$

$$O_2(a) + I_2(A', A) \rightarrow O_2(X) + 2I \tag{25}$$

The lowest electronically excited states of I_2 are $A'^3\Pi_{2u}$ and $A^3\Pi_{1u}$ with excitation energies 10,047 cm^{-1} and 10,847 cm^{-1}, respectively. The energy gaps between $O_2(a)$ and $I_2(A'$ or $A)$ are much greater than thermal collision energies. Therefore the electronic–electronic (EE) energy transfer rate from $O_2(a)$ cannot account for the observed I_2 dissociation rate using the combination of reactions (19) and (25). However, electronically excited $I_2(A', A)$ is readily observed in $O_2(a)/I_2$ mixtures.[13–16] David[14] studied the I_2A–X emission when molecular iodine was added to a flow of singlet oxygen. Heidner et al.[13] also recorded the I_2 $A \rightarrow X$ emission spectrum from an $O_2(a)/I_2$ gaseous mixture. The lowest energy electronically excited state of $I_2(A')$ is very metastable and cannot be detected by emission spectroscopy. Nota et al.[16] have demonstrated that $I_2(A')$ is produced in $O_2(a)/I_2$ mixtures using laser-induced-fluorescence detection of the D'–A' transition.

The mechanisms by which the I_2A' and A states are populated in $O_2(a)/I_2$ mixtures have not been established. One possibility is that the energy defect for reaction (19) is overcome by vibrational excitation of $O_2(a)$. In support of this mechanism, vibrationally excited oxygen has been observed in flows of singlet oxygen. Browne and Ogryzlo[17] observed emissions from $O_2(a, v = 1)$ and $O_2(b, v = 1)$ from the reaction zone of a bubble-type singlet oxygen generator. Lilenfeld[4] detected vibrationally excited oxygen in the flow from singlet oxygen generator using electron paramagnetic resonance spectroscopy. Recent studies[18,19] have shown that a nonequilibrium population of O_2 vibrational levels occurs in singlet oxygen–iodine mixtures. Approximately 2% of $O_2(a)$ at the output of a chemical singlet oxygen generator was found to be in the first vibrationally excited level,[18] and more than 20% of the oxygen molecules are vibrationally excited in the COIL active medium.[19] The O_2 vibrational energy can have a substantial effect on the dissociation of molecular iodine. The energy gaps in process (95) (see Table 1; Refs. 20–28), 623 cm^{-1}, and in process (96), 23 cm^{-1}, are within reach for thermal collisions. In this case the rates of these reactions can be fast enough to provide the observed I_2 dissociation rate. For $O_2(a)$ in vibrational level, $v = 3$, the available energy is enough to dissociate I_2 in a single collision[29] (process 97). A model of this kind was advanced by Lilenfeld[4] in 1983, and recent experimental studies[6,14–19] provide new indications that electronically excited I_2 is the critical dissociation intermediate. At present, the kinetic data needed to further test the validity of this mechanism are not available.

In the work described here we have examined the preceding two alternative descriptions of the iodine dissociation process. The possible role of $O_2(b)$ as the initiator of the sequence was examined using flow-tube techniques with singlet oxygen from a jet-type chemical generator. To explore the role of electronically excited I_2, a

Table 1 Additional reactions for vibrationally excited O_2 in COIL

No.	Reaction	Rate constant, cm^3/s	Ref. no.
9	$O_2(b) + CO_2 \rightarrow O_2(a,v) + CO_2(v')$	4.2×10^{-13}	21
28	$I_2(A') + O_2(X) \rightarrow I_2(X) + O_2(a)$	6.3×10^{-12}	20
29.1	$I_2(A') + H_2O \rightarrow I_2(X) + H_2O$	3.4×10^{-12}	20
29.2	$I_2(A') + N_2 \rightarrow I_2(X) + N_2$	3.5×10^{-14}	22
29.3	$I_2(A') + CO_2 \rightarrow I_2(X) + CO_2$	8.5×10^{-13}	This work
29.4	$I_2(A') + He \rightarrow I_2(X) + He$	9.4×10^{-15}	22
70	$O_2(v) + O_2 \rightarrow O_2(v-1) + O_2$	8.2×10^{-19}	23
71	$O_2(v) + H_2O \rightarrow O_2(v-1) + H_2O$	8.2×10^{-17}	24
72	$O_2(v) + He \rightarrow O_2(v-1) + He$	0	——
73	$O_2(v) + N_2 \rightarrow O_2(v-1) + N_2$	0	——
76	$O_2(X, 2) + O_2(X, 0) \rightarrow O_2(X, 1) + O_2(X, 1)$	2.0×10^{-13}	25
77	$O_2(X, 3) + O_2(X, 0) \rightarrow O_2(X, 2) + O_2(X, 1)$	2.6×10^{-13}	25
78	$O_2(X, 4) + O_2(X, 0) \rightarrow O_2(X, 3) + O_2(X, 1)$	2.7×10^{-13}	Calculated
79	$O_2(a, 1) + CO_2 \rightarrow O_2(a,0) + CO_2(v)$	1.8×10^{-14}	26
80	$O_2(a, 2) + CO_2 \rightarrow O_2(a, 1) + CO_2(v)$	4.4×10^{-14}	26
81	$O_2(a, 3) + CO_2 \rightarrow O_2(a, 2) + CO_2(v)$	1.0×10^{-13}	Calculated
82	$O_2(b, 1) + CO_2 \rightarrow O_2(b, 0) + CO_2(v)$	1.2×10^{-12}	21
83	$O_2(b, 2) + CO_2 \rightarrow O_2(b, 1) + CO_2(v)$	1.7×10^{-12}	21
84	$O_2(b, 3) + CO_2 \rightarrow O_2(b, 2) + CO_2(v)$	1.6×10^{-12}	21
85	$O_2(X, 1) + H_2O(000) \rightarrow O_2(X, 0) + H_2O(010)$	1.7×10^{-12}	27
89	$O_2(a, 1) + O_2(X, 0) \rightarrow O_2(X, 1) + O_2(a, 0)$	5.6×10^{-11}	26
90	$O_2(a, 2) + O_2(X, 0) \rightarrow O_2(X, 2) + O_2(a, 0)$	3.6×10^{-11}	26
91	$O_2(b, 1) + O_2(X, 0) \rightarrow O_2(X, 1) + O_2(b, 0)$	1.52×10^{-11}	21
92	$O_2(b, 2) + O_2(X, 0) \rightarrow O_2(X, 2) + O_2(b, 0)$	1.7×10^{-12}	21
93	$O_2(b, 3) + O_2(X, 0) \rightarrow O_2(X, 3) + O_2(b, 0)$	1.5×10^{-13}	21
94	$H_2O(010) + H_2O \rightarrow H_2O(000) + H_2O$	5×10^{-11}	28
95	$O_2(a, 1) + I_2(X) \rightarrow O_2(X) + I_2(A')$	2×10^{-12}	Parameter
96	$O_2(a, 2) + I_2(X) \rightarrow O_2(X) + I_2(A)$	3×10^{-11}	Parameter
97	$O_2(a, 3) + I_2(X) \rightarrow O_2(X) + I + I$	10^{-11}	Parameter

laser pump-probe technique was used to measure relaxation rate constants for $I_2(A')$. Based on the results from these experiments, we have proposed a kinetic model for the dissociation that involves vibrationally excited $O_2(a)$ and electronically excited I_2.

II. Kinetic Studies of I_2 Dissociation in Flowing $O_2(a)/H_2O/I_2/CO_2$ Mixtures

A. Experiment

The low-pressure flow cell apparatus used to study the I_2 dissociation rate is shown schematically in Fig. 1. Details of this system are described in Refs. 19 and 30. The dissociation process was followed indirectly by observing the emissions from the excited species I^*, $O_2(b)$ and $I_2(B)$. Emission intensities were measured as a function of distance along the flow tube (equivalent to reaction time). To facilitate these measurements, the detectors (Si and Ge photodiodes) and an optical fiber (13) were mounted on a movable platform (10). A jet-type chemical singlet oxygen generator (SOG) (1) was used to produce $O_2(a)$. The counterflow jet-type SOG reaction zone consisted of a cylindrical cavity 12 mm in diameter and 10 cm height, which was drilled through a block of Plexiglas®. Gaseous Cl_2 was injected into the lower part of a reaction zone through two opposing inlets. Basic hydrogen-peroxide (BHP) solution was injected at the top of the reaction zone. The BHP injector consisted of 43 stainless-steel tubes, each with an inner diameter of 0.5 mm and length of 25 mm. The jets and the gas flow velocities in the reactor were 5 and 12 m/s, respectively. The BHP solution was prepared from 1.2 liters of H_2O_2 (37% weight) and 0.8 liters of solution KOH (14.5 mole/liter). The solution temperature was maintained -15°C.

N_2 or CO_2 was used as a carrier gas for iodine vapor. Gaseous molecular iodine was produced in a vapor generator where it was mixed with the carrier gas. The resulting mixture was then passed through a diagnostic cell where an optical absorption measurement was used to determine the I_2 partial pressure P_{I_2}. The absorbance at a wavelength of 500 nm was used for this purpose. The I_2 flow rate was derived from the ratio $G_{I_2} = G^s_{\text{buf}} P_{I_2}/P_{\text{buf}}$. The relative iodine molecule density was obtained from the expression $\eta_{I_2} = G_{I_2}/G_{Cl_2}$.

A low-pressure flow cell made of Plexiglas was attached directly to the exit of the SOG. The gas flow channel had a cross section of 5×1.5 cm. The gaseous $I_2/N_2/CO_2$ mixture was injected into the flow cell through nine iodine nozzles (4). Nozzle height, width, and length along the flow were 1.5 cm, 2.5 mm, and 1.0 cm, respectively; the thickness of the copper walls of the nozzles was 0.15 mm. The distance between lateral surfaces of adjacent nozzles was 2.5 mm.

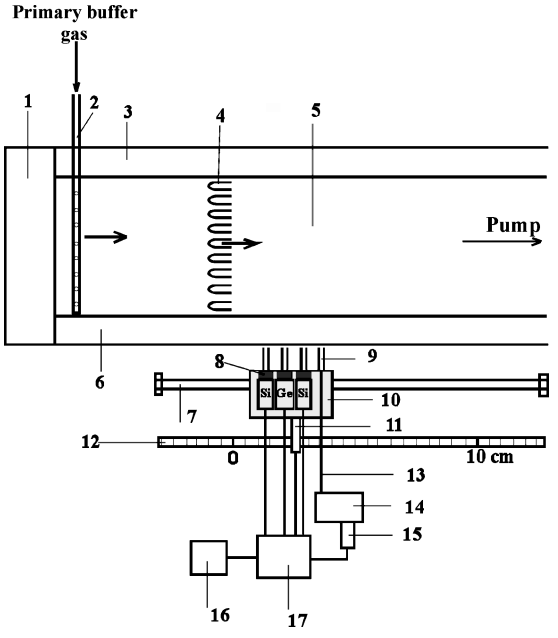

Fig. 1 Upper view of the low-pressure flow cell apparatus: 1, jet SOG; 2, port for input of primary buffer gas; 3 and 6, walls of measuring cell; 4, secondary buffer gas and iodine nozzles; 5, gas duct with cross section 1.5 × 5 cm²; 7, movable platform director; 8, optical filters; 9, visual angle tube; 10, movable platform; 11, slider; 12, scale, 13, optical multiple fiber; 14, monochromator; 15, photomultiplier; 16, PC; 17, analog-digital converter; and Si and Ge, photodetectors.

Flat, parallel jets of oxygen were formed in the section of the gas channel that was not obscured by the iodine nozzles (4). Hence, the nozzles formed alternating iodine and oxygen gas jets with identical cross sections of 2.5×15 mm. The temperature of the nozzles was maintained at 40°C to avoid condensation of iodine on their walls. The primary [port (2)] and secondary buffer gases flow rates were metered by a flowmeter. The molecular iodine mole fraction was varied by altering the fraction of buffer gas bypassed around the I_2 vapor generator.

Optical emissions were observed through the wall of the measuring cell (6). Optical filters were used to limit the range of wavelengths observed by each detector. The $I^* \rightarrow I$ emission was detected by the Ge photodiode. A long-pass filter installed in front of the diode blocked the visible emissions from the reactants in the flow-tube. Visible $I_2 \rightarrow B$–X emission was detected by the Si photodiode, which was equipped with a ≤600-nm short-pass filter. The $I_2 B$–X emission is spread over a wide spectral range, and the tail of this emission overlaps the O_2 $b \rightarrow X$ band. Consequently, the $I_2(B)$ and $O_2(b)$ emissions near 762 nm cannot be separated using optical filters. The monochromator (14) was used for this purpose. Tubes (9) with inner diameter of 4.5 mm and length of 35 mm specified the observation angle such that the observation region in measuring cell can be approximated by a cylinder with a diameter of 1 cm. Optical emission was transported by an optical multiple fiber (13) to the entrance slit of the monochromator (14) and detected by a photomultiplier (15). A precise dc amplifier whose frequency response extended from 0 to 10 Hz amplified the photomultiplier signal.

The gas stream from the SOG consisted of oxygen, residual chlorine, water vapor, and the primary buffer gas introduced through port (2). The secondary gas stream supplied to the measuring cell through nozzles (4) consisted of molecular iodine vapor entrained in the carrier gas. In all experiments the flow rates of the primary and the secondary gas streams were identical. Therefore, the velocities of the gas jets after the nozzles can be considered approximately equal to each other. In all experiments the Cl_2 flow rate was held constant at $G_{Cl_2} = 2.5$ mmole/s. The primary buffer gas flow rate was adjusted to meet the condition $G^p_{\text{buf}} = (G_{\text{buf}} - G_{Cl_2})/2$, where $G_{\text{buf}} = G^p_{\text{buf}} + G^s_{\text{buf}}$ was the total buffer gas flow rate. The $O_2(a)$ yield in the SOG output was $\eta_a = N_a/N_{O_2} \approx 60 \pm 10\%$. Cl_2 utilization in the generator exceeded 95%.

For the experimental conditions of this study, the characteristic distance for the mixing zone along the flow is given by $l_{\text{mix}} \approx d^2_{\text{mix}} U/D \approx 1$ cm, where $d_{\text{mix}} \approx 1.2$ mm is for mixing scale transverse to the flow direction, $U \approx 60$–70 m/s is the gas velocity. Diffusion of the iodine molecules in oxygen–iodine mixture at gas pressures near $P = 1$ torr (Ref. 31) was governed by the diffusion coefficient $D = D_0/P$ with $D_0 = 57$ cm²/s . The extent of the iodine dissociation zone along the flow l_{dis} depends strongly on the initial I_2 content. For our experimental conditions it was $l_{\text{dis}} \geq 5$ cm. All of the reported measurements were made under conditions where $l_{\text{dis}} \gg l_{\text{mix}}$. Most of measurements were carried out at the relative initial I_2 density $\eta_{I_2} \cong 0.3\%$, where the I_2 dissociation zone was close to 12 cm. The cross sections and gas velocities of iodine and oxygen streams at the exit of iodine nozzles were the same. Hence, the local initial I_2 concentration in the iodine stream prior to mixing was only a factor of two higher than in the completely mixed flow.

We used the same procedure as Heidner et al.[32] to determine the absolute I^* concentration. This was evaluated by comparing the emission intensities at 1315 nm ($I^* \rightarrow I$) and 1268 nm [$O_2(a) \rightarrow O_2(X)$]. The oxygen gas stream produced in the SOG with a known oxygen content was passed through the measuring cell. For this situation the Ge photodiode signal corresponds to $I_{\text{Ge}} = C \cdot A_{1268} N_a = C \cdot A_{1268} P_c \eta_a/(kT)$. Using that $A_{1268} = 2.19 \times 10^{-4}$ s^{-1} (Ref. 33) and assuming that the $O_2(a)$ yield at the exit of the SOG was 60%, we found the detectivity correction coefficient C from this expression for our experimental conditions. Taking into account the Einstein coefficient for $I^* \rightarrow I$ transition of

$A_{1315} = 7.8\ s^{-1}$, the absolute I* concentration is given by the ratio $N_{I^*} = I_{Ge}/(C \cdot A_{1315})$.

B. Experimental Results

1. Profiles of I Concentrations*

Figure 2 shows plots of the excited iodine atom distributions along the flow for the different dilutions of oxygen by a) nitrogen and b) by carbon dioxide at relative water vapor concentration of $\eta_w = N_w/N_{O_2} = 3\%$, and relative iodine vapor content $\eta_{I_2} = 0.28\%$. One can see from Fig. 2a that the maximum concentrations of atomic I* were almost unaffected using dilution ratios up to N_2:$O_2 = 3$:1. The locations of these maxima shifted downstream as the dilution ratio increased. This was primarily caused by the influence of buffer gas dilution on the gas flow velocity. The gas velocity distribution in the measuring cell depends on the local temperature. Buffer gas dilution decreases the temperature increase associated with the reactive heat release, such that the initial gas velocity can be calculated from the expression

$$U_0(\text{m/s}) = \frac{0.62 \cdot T_0 G_{Cl_2}(\text{mmole/s}) \sum_i \eta_i}{P_c(\text{torr}) H(\text{cm}) \cdot B(\text{cm})}$$

where

$$\sum_i \eta_i = \sum_i \frac{G_i}{G_{Cl_2}}$$

For example at the initial gas temperature $T_0 = 300$ K the gas velocity calculated under conditions of Fig. 2a for the mixture N_2:$O_2 = 1$:1 is 62 m/s, and for the mixture N_2:$O_2 = 3$:1 is 69 m/s.

The dependence of the I* concentration on the downstream distance and CO_2 buffer gas dilution is shown in Fig. 2b. The maxima of the excited iodine atom distributions are shifted downstream with increasing dilution level, to an extent that is clearly greater than shift caused by N_2 dilution. This implies that the addition of CO_2 reduces the I_2 dissociation rate. It is well known that the I_2 dissociation rate accelerates with increasing η_{I_2}. Consequently, it is expected that the influence of CO_2 gas will diminish as η_{I_2} is increased. Figure 3 shows the effect of CO_2 on I* formation for $\eta_{I_2} = 0.93\%$. The shifts of the maxima along the flow direction are less pronounced for these conditions and can be explained by the heat capacity effect. The gas

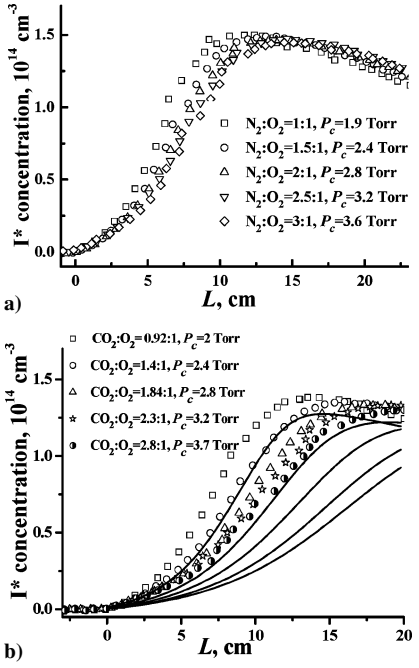

Fig. 2 I* atom concentrations vs downstream coordinate L for $\eta_{I_2} = 0.28\%$ and $\eta_w = 3\%$. The effect of adding N_2 or CO_2 buffer gases is shown in plots a and b, respectively. The smooth curves are simulations based on the kinetic model of Derwent and Thrush[7] and Derwent et al.[8]

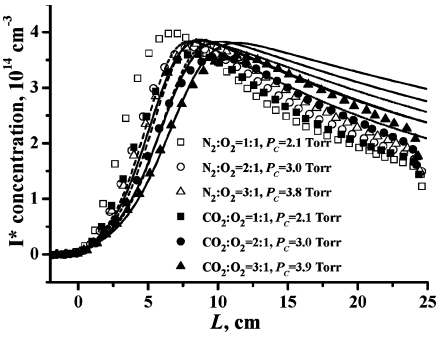

Fig. 3 I* atoms concentration vs downstream coordinate L for $\eta_{I_2} = 0.93\%$ and $\eta_w = 3\%$. Data points are shown for varies dilutions of oxygen by N_2 or CO_2 buffer gas. The curves are the simulated I* atom profiles for the advanced $I_2(A', A)$ dissociation model at the conditions as for experimental one. The broken and solid lines are for dilution by N_2 and CO_2 , respectively. Lines are displaced at the right at increase of dilution by buffer gas.

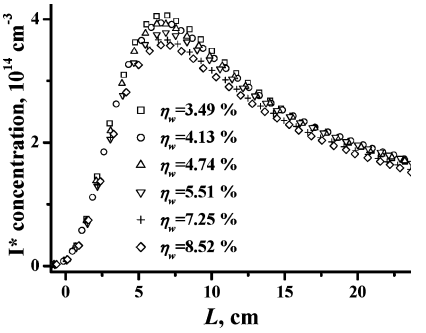

Fig. 4 Dependence of the I* concentration on the distance along the flow for $P_c = 2$ torr, O_2:$N_2 = 1$:1, $\eta_{I_2} = 1\%$.

mixture for Fig. 3 is close to that used in COIL. Note that these flow-tube observations support the conclusion of Ref. 34 that CO_2 can be used to replace N_2 as an inexpensive buffer gas for COIL.

The effect of H_2O on the dissociation rate is similar to that of CO_2. For higher η_{I_2} and yield of singlet oxygen, the influence of water vapor on the I_2 dissociation rate becomes less important. Figure 4 represents the dependence of the I* concentration on the downstream distance for $\eta_{I_2} = 1\%$ with relative water vapor concentrations lying in the range 3.5–8.5%. The strong dependence of I_2 dissociation rate on H_2O found in earlier flow tube experiments[13] can be explained by the small singlet oxygen yield (10%) of the generators used. As can be seen from Fig. 4, the influence of water vapor on the I* distributions was insignificant for the present experimental conditions. Khvatov et al.[35] observed that the gain coefficient in COIL depends weakly on the water vapor content for conditions that were similar to those of the measurements presented in Fig. 4. Hence, the flow-tube experiments confirm the conclusion of Ref. 35.

2. Profiles of $O_2(b)$ Concentrations

CO_2 is a suitable agent to test the role of $O_2(b)$ because it is good quencher for $O_2(b)$ ($K_9 = 4.2 \times 10^{-13}$ cm^3 s^{-1}), although it is not effective in quenching $O_2(a)$ or I*. The addition of CO_2 is expected to reduce the I_2 dissociation rate if $O_2(b)$ plays an active role in this process. The O_2 b–X emission bands are observed near 762 nm, in the long-wavelength tail of the $I_2B \rightarrow X$ system.[19] However, the Einstein coefficient for the I_2 emission is orders of magnitude greater than that of the O_2 b–X system. As a consequence, although the concentration of $I_2(B)$ is very small the I_2B–X and O_2 b–X emissions are seen with comparable intensities near 762 nm at the start of the dissociation process. The temporal profiles of the $I_2(B)$ and $O_2(b)$ emissions are significantly different. This is evident in Fig. 5, which shows the 762-nm emission intensity profiles for flows with η_{I_2} in the range 0.18–0.94%. When η_{I_2} is greater than 0.5%, there are two intensity maxima in the traces. The first maximum is produced by the I_2 B–X emission band. The radiation from this

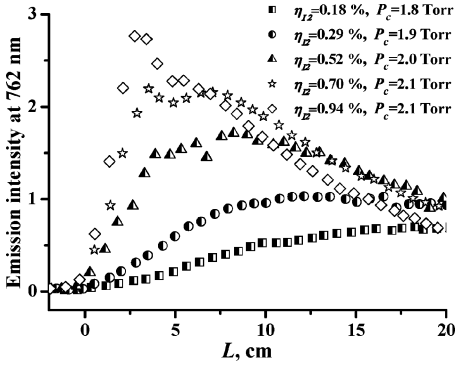

Fig. 5 Dependence of the 762-nm emission intensity as a function of distance along the flow for $\eta_w = 3\%$, O_2:N_2 = 1:1.

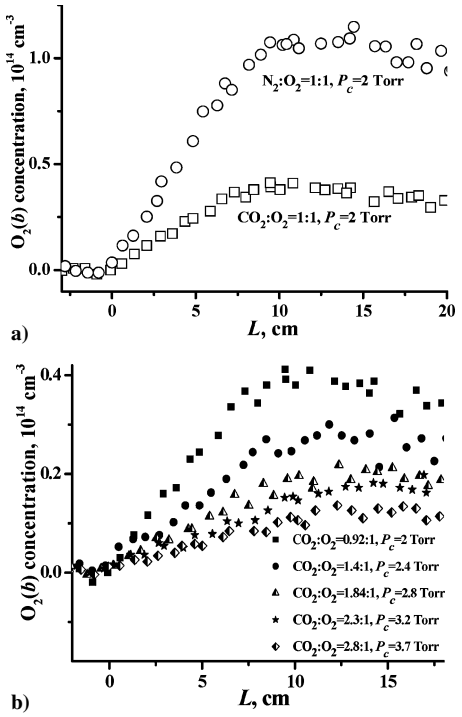

Fig. 6 Dependence of $O_2(b)$ concentrations on the distance along the flow for $\eta_w = 3\%$ and $\eta_{I_2} = 0.28\%$ with N_2 (upper plot in panel a) and CO_2 buffer gas dilutions.

transition decreases quickly along the flow, and its contribution becomes insignificant after the I_2 dissociation zone. We found that the contribution of the I_2 $B \rightarrow X$ emission near $\lambda = 762$ nm was negligible compared to the O_2 b–X emission for $\eta_{I_2} < 0.5\%$ at all distances along the flow cell.

The plots shown in Fig. 6 demonstrate the loss of $O_2(b)$ that occurs when CO_2 is added to the gas flow. These measurements were performed with $\eta_{I_2} = 0.28\%$, so that the 762-nm emission could be used to determine the $O_2(b)$ concentration without interference from $I_2(B)$. In Fig. 6 it can be seen that the $O_2(b)$ concentration was reduced from $N_b \approx 1.1 \times 10^{14}$ cm^{-3} (upper trace of Fig. 6a) to $N_b \approx 1.3 \times 10^{13}$ cm^{-3} (the bottom trace of Fig. 6b) by the addition of 2.7 torr of CO_2. Despite this dramatic loss of $O_2(b)$, Figs. 2 and 3 show that the addition of this quantity of CO_2 had very little influence on the I_2 dissociation rate.

3. Profiles of the I_2 $B \rightarrow X$ Emission Intensity

The I_2 $B \rightarrow X$ emission in the 480–600-nm wavelength range was monitored using the Si photodetector. The relative intensity of this emission along the flow is shown in Fig. 7a for N_2 buffer gas and in Fig. 7b for CO_2 buffer gas. The increase of either N_2 or CO_2 buffer gas pressure decreased the $I_2B \rightarrow X$ emission intensity. In Fig. 7a it

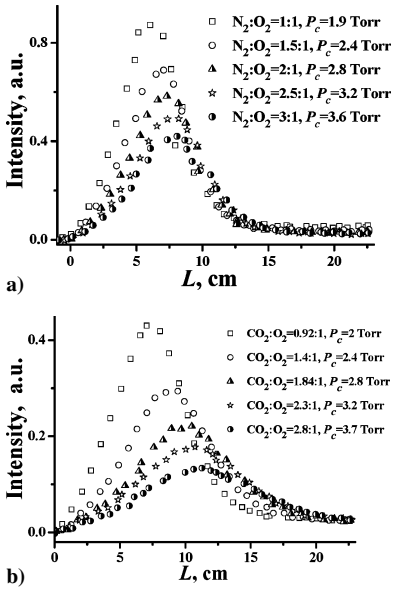

Fig. 7 I_2 B–X emission intensity of an oxygen-iodine mixture diluted by a) N_2 and b) CO_2 buffer gas as a function of downstream coordinate L at $\eta_w = 3\%$, $\eta_{I_2} = 0.28\%$.

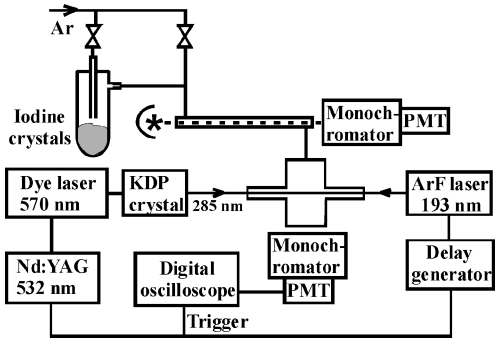

Fig. 8 Schematic view of the laser pump-probe apparatus.

can be seen that the maximum intensity of the $B \rightarrow X$ emission was inversely proportional to the N_2 partial pressure. This is attributed to rapid removal of $I_2(B)$ by induced-collision predissociation. CO_2 is good quencher for both $O_2(b)$ and $I_2(B)$, where the rate constant for collision-induced dissociation by CO_2 is close to gas kinetic. Because of this circumstance, the intensity of the $I_2B \rightarrow X$ emission band should be inversely proportional to the square of the partial pressure of carbon-dioxide gas P_{CO_2} if the $I_2(B)$ is populated in a reaction sequence involving $O_2(b)$ and $I_2(A)$, as proposed by Derwent and Thrush.[7] The observed dependence was slightly greater than linear ($I_{B-X} \propto P_{CO_2}^{-1.1}$; compare to Fig. 7b), indicating that $O_2(b)$ plays an insignificant role in the excitation the I_2B state.

III. Energy-Transfer Kinetics of the A′ State of I_2

A. Experiment

The deactivation of $I_2(A')$ by CO_2, Ar, and I_2 was examined using a laser pump-probe technique. Figure 8 shows a schematic diagram of the apparatus used for these measurements. UV excitation of I_2 diluted in Ar was used to populate the A' state via an indirect pathway. An ArF excimer laser operating at 193 nm (Lumonics TE-860-4, pulse duration 10 ns) was used to excite the $I_2D(0_u^+) \leftarrow X$ transition. Collisions with Ar rapidly induced transfer to the $D'(2_g)$ state, which then radiated down to populate the A' state.[36] Population transfer was complete within 100 ns after the laser pulse. The time evolution of the $I_2(A')$ was followed by using delayed pulses from a tunable dye laser to reexcite the D'–A' transition.[36] The output from the dye laser was frequency doubled to obtain tunable light at wavelengths near 285 nm. The delay between the laser pulses was

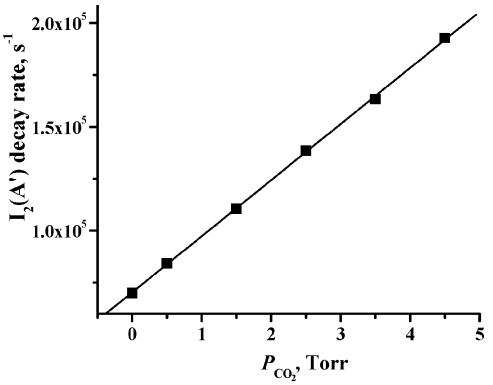

Fig. 9 Dependence of the $I_2(A')$ decay rate on CO_2 partial pressure at $P_{Ar} = 50$ torr, $P_{I_2} = 0.013$ torr and $T = 300$ K.

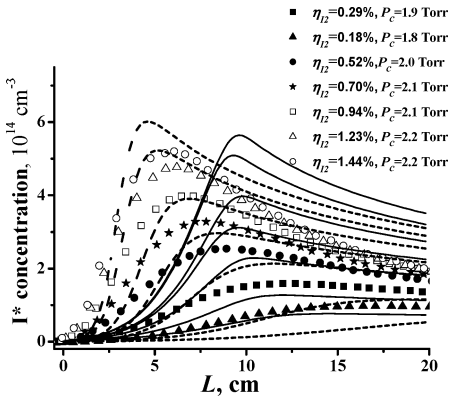

Fig. 10 Dependence of the I^* concentration on the distance along the flow for $\eta_w = 3\%$, O_2:N_2 = 1:1. The broken curves are simulations for the standard dissociation model, modified by allowing initiation by $O_2(b)$. The smooth curves are simulations based on the kinetic model of Derwent and Thrush[7] and Derwent et al.[8] Lines are displaced at the right at increase of η_{I_2}.

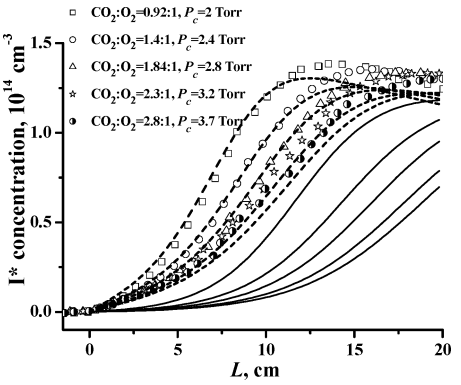

Fig. 11 Dependence of the I^* concentration on the distance along the flow for $\eta_w = 3\%$, $\eta_{I_2} = 0.28\%$. The broken curves are simulations for the advanced $I_2(A', A)$ dissociation model at the conditions as for experimental one. The smooth curves are simulations for the standard dissociation model, modified by allowing initiation by $O_2(b)$. Lines are displaced at the right at increase of dilution by CO_2 buffer gas.

controlled by a precision delay generator (SRS model DG 535). I_2 $D' \rightarrow A'$ fluorescence at $\lambda = 340$ nm was selected by a 0.25 M monochromator and detected by a photomultiplier (PMT). The PMT signal was captured by a LeCroy digital oscilloscope.

The fluorescence cell was constructed from a six-way cross. The cell was evacuated by a rotary pump, and the pressure was measured using capacitance manometers (MKS Baratron Models 622, 0–1000 torr, and 122A, 0–10 torr). I_2 was seeded in the carrier gas flow by passing Ar over I_2 crystals at ambient temperature. Needle valves were used to control the gas flow rates. The optical absorption at 500 nm was used for I_2 concentration measurements. The I_2 and carrier gas mixture was passed through a 1.2-m-long absorption cell immediately before entering the fluorescence cell. Metered quantities of quenching gases were added to the I_2/Ar mixture to observe the quenching kinetics.

B. Results

To test the apparatus we reexamined the quenching of $I_2(A')$ by Ar and I_2. The rate constants obtained, 2.7×10^{-14} cm^3/s for Ar and 4.8×10^{-11} cm^3/s for I_2, were in good agreement with the values reported in Ref. 36. Measurements of the $I_2(A')$ decay as a function of the CO_2 partial pressure are presented in Fig. 9. The rate constant for quenching of $I_2(A')$ by CO_2 defined by this plot is $K_{CO_2} = 8.5 \times 10^{-13}$ cm^3/s. The rate constant for quenching by O_2 reported in Ref. 20 ($K_{O_2} = 6.3 \times 10^{-12}$ cm^3/s) is much greater than the rate constants for quenching by CO_2 or H_2O ($K_{H_2O} = 3.4 \times 10^{-12}$ cm^3/s from Ref. 28). This supports the notion that O_2 quenches $I_2(A')$ by an E-E transfer process of the form $I_2(A') + O_2(X) \rightarrow I_2(X) + O_2(a)$, where the products can be vibrationally excited. This process, which is the reverse of the $I_2(A')$ excitation mechanism considered in the Introduction, has been observed in cryogenic Ar matrices[15] that were doped with I_2 and O_2.

IV. Kinetic Modeling of the I_2 Dissociation Process in the COIL Active Medium

In reevaluating the role of $O_2(b)$ in the dissociation mechanism, we began by reexamining the Derwent and Thrush[7] and Derwent et al.[8] model, where $O_2(b)$ is the dissociation agent. In the analysis of their flow-tube experiments, Heidner et al.[13] noted that the Derwent and Thrush[7] and Derwent et al.[8] model could reproduce the rate of I_2 dissociation rate over the range of conditions achieved in their experiments, where the $O_2(a)$ yield did not exceed 10%. In the present work we have expended the range of experimental conditions by using higher singlet oxygen yields and CO_2 as a buffer gas. Calculations based on the Derwent and Thrush model are represented in Figs. 2b and 10, with the assumption of a gas kinetic rate constant for reaction $21 - K_{21} = 3 \times 10^{-10}$ cm^3/s. One can see from Fig. 10 that the predicted maximum I^* concentrations are in agreement with the experimental data. However the locations of the maxima are shifted downstream at the higher I_2 concentrations. In Fig. 2b it can be seen that the calculated I_2 dissociation rates depended strongly on the CO_2 concentration caused by rapid quenching of $O_2(b)$ [reaction (9) from Table 1]. These results clearly demonstrate direct dissociation by $O_2(b)$ is unimportant as a primary dissociation channel.

As noted in the Introduction, we were interested in the possibility that reaction (21) could be fast enough to be the initiation step for the dissociation process. A model that relied on reaction (21) for initiation was examined. Reaction (32) was removed from the standard package, and the rate constant for reaction (21) was set to the recently reported[11] value of $K_{21} = 3 \times 10^{-11}$ cm^3/s. The rate constants for vibrational deactivation of $I_2^\dagger$ were fixed at the values reported in Ref. 3 (H_2O, 1.3×10^{-11} cm^3/s; O_2, 5.6×10^{-12} cm^3/s). The rate constant for deactivation by CO_2 has not been determined, but it is expected that it will be similar to that of O_2. Hence, the rate constant for this process was set to 6×10^{-12} cm^3/s. With $I_2^\dagger$ as the primary intermediate, the rate of dissociation is strongly dependent on the $\gamma_{33, v>20}$ excitation probability. This was treated as a variable parameter, as was the rate constant for dissociation $I_2^\dagger$ of $O_2(a)$ [reaction (34)]. A satisfactory level of agreement between simulations based on this model and the experimental data could not be achieved. The closest match was obtained using $\gamma_{33, v>20} = 0.4$ and $K_{34} = 1 \times 10^{-10}$ cm^3/s. The simulations for these parameters are shown in Figs. 10 and 11, where the defects of the model are obvious. Clearly, the influence of CO_2 quenching is too great with this reaction mechanism.

An alternative I_2 dissociation model was constructed in which the intermediate electronically excited states of I_2 are populated by collisions with vibrationally excited singlet oxygen molecules. The standard COIL kinetics package[2] was augmented by the reactions

listed in Table 1, and the standard reactions (32), (34–36) were eliminated. The key modification of the revised model is excitation of the I_2A' and A states by collisions with vibrationally excited singlet oxygen molecules [processes (95–97) in Table 1]. The excited intermediate is then dissociated by the step $O_2(a) + I_2(A' \text{ or } A) \rightarrow O_2(X) + 2I$ [reaction (25)]. Reactions describing O_2 vibrational excitation and relaxation kinetics in COIL are an essential component of the new model. A distinctive feature of O_2 is that its vibrational energy is not easily lost through vibrational–translational (VT) collisional relaxation [processes (70–73)]. The primary relaxation process for vibrationally excited O_2 in the COIL system is vibrational–vibrational (VV) transfer in collisions with H_2O [reaction (85)]. This energy is subsequently transferred to the thermal bath by VT relaxation of the H_2O via reaction (94). In this model we took into account the fact that the VV energy exchange between stretching and bending H_2O modes occurs much faster than the VT relaxation of stretching modes. Because of this, vibrational energy quanta in the water molecules are accumulated predominantly in the bending mode.

Vibrationally excited O_2 in the COIL active medium can be generated by the electronic deactivation processes (1), (3), (5), (44), and (45) presented in standard COIL kinetics package[2] and, when CO_2 is present, reaction (9) in Table 1. Unfortunately, there is very little information concerning the final state distributions of these reactions. Antonov et al.[37] and Azyazov et al.[38] estimated that 4.5 vibrational quanta of oxygen are produced in the COIL active medium for the deactivation one singlet oxygen molecule in processes (1), (3), (5), (9), (44), and (45), based on comparisons of experimental and calculated results. This indicates that the majority of the energy released in the electronic relaxation process appears as O_2 vibrational energy. In the present model we have defined the distributions resulting from electronic to vibrational energy-transfer processes using fractional scaling coefficients denoted by $\gamma_{i,j}$. These specify the probability that the jth vibrational level of O_2 is excited by the ith reaction. We chose the values of $\gamma_{i,j}$ such that the number of vibrational quanta formed by the quenching of one $O_2(a)$ molecule does not exceed 4.5. The following values for the coefficients were assumed: $\gamma_{1,1} = 0$; $\gamma_{1,2} = 1$; $\gamma_{3,3} = 1$; $\gamma_{5,1} = 0$; $\gamma_{5,2} = 0$; $\gamma_{5,3} = 1$; $\gamma_{9,1} = 0$; $\gamma_{9,2} = 0$; $\gamma_{9,3} = 1$; $\gamma_{44,1} = 0$; $\gamma_{44,2} = 1$; $\gamma_{45,1} = 0$; $\gamma_{45,2} = 0$; $\gamma_{45,3} = 1$. It has been shown theoretically[19] that the vibrational population distributions of $O_2(X)$, $O_2(a)$, and $O_2(b)$ are approximately equal because of fast EE energy exchange between oxygen molecules [processes (89)–(92)]. VV exchange rate constants $K_{v',v''}$ for the processes $O_2(v') + O_2(v'') \rightarrow O_2(v'-1) + O_2(v''+1)$ are known only for a small range of vibrational levels. Coletti and Billing[39] calculated the value of $K_{1,0}$ to be close to 10^{-13} cm^3/s. Kalogerakis et al.[25] reported experimental values of $K_{2,0} = 2 \times 10^{-13}$ cm^3/s, and $K_{3,0} = 2.6 \times 10^{-13}$ cm^3/s. All other $K_{v',v''}$ were calculated them from the expression[40]: $K_{v',v''} = 10^{-13}(v'+1)v'' \exp[-\delta_{VV}|v'+1-v''|][1.5–0.5 \exp(-\delta_{VV}|v'+1-v''|)]$ cm^3/s, where $\delta_{VV} = 0.4(300/T)^{\frac{1}{2}}$. The initial relative populations of vibrationally excited oxygen were calculated as in Ref. 41.

Calculations of I* atom concentrations using the revised model are shown in Figs. 11 and 12. The dissociation channel of reaction (21) with the new value of the rate constant measured in Ref. 11 was also taken into account. The calculated profiles of I* atom concentrations are in good agreement with the experimental data. The shift of the calculated I* concentration peaks along the flow in Fig. 11 is caused by quenching of vibrationally excited O_2 in processes (79–84).

V. Discussion

The experimental results obtained in this study indicate that direct dissociation of I_2 by $O_2(b)$ [reaction (21)] is unimportant in the COIL dissociation mechanism. As expected, simulations that used the Derwent and Thrush[7] and Derwent et al.[8] mechanism were markedly influenced by CO_2 quenching of $O_2(b)$. The model in which reaction (21) replaces reactions (32) and (34) for the initial production of I atoms was also found to be inconsistent with the observed kinetics in the presence of CO_2 buffer gas. Again the simulations predicted a strong dependence on the CO_2 partial pressure that was not reflected by the experimental data. In essence

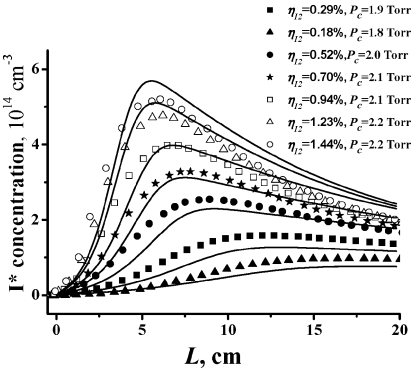

Fig. 12 Dependence of the I* concentration on the distance along the flow for $\eta_w = 3\%$, O_2:N_2 = 1:1. The smooth curves are simulations for the advanced $I_2(A',A)$ dissociation model at the conditions as for experimental one. Lines are displaced at the right at increase of η_{I_2}.

these models fail because the dissociation rate begins to fall when $K_9[CO_2]$ becomes comparable to $K_{21}[I_2]$ (i.e., $[CO_2]/[I_2] > 70$).

The dissociation model that agrees with the present data is that of Antonov and coworkers.[42] This involves excitation of $I_2(A', A)$ by vibrationally excited $O_2(a)$ as a critical step. $I_2(A', A)$ is then dissociated by a subsequent collision with $O_2(a)$. Given that the rate constant reported here for quenching of $I_2(A')$ by CO_2 is relatively large (8.5×10^{-13} cm^3 s^{-1}), it might seem surprising that that this model is not very sensitive to this process. The key to understanding this behavior is to recognize that quenching of $I_2(A', A)$ must compete with the rapid dissociation of $I_2(A', A)$ by $O_2(a)$. Deactivation of $I_2(A', A)$ by CO_2 will become significant when $K_{29,3}[CO_2]$ is comparable to $K_{25}[O_2(a)]$. Assuming a gas kinetic rate constant for reaction 25 implies that electronic quenching by CO_2 will become influential when $[CO_2]/[O_2(a)] > 300$. The conditions of the experiments reported here did not approach this ratio.

In contrast with the standard mechanism, the model presented here does not assign a significant role to vibrationally excited $I_2(X)$. However, the studies of Hall et al.,[43] Van Bentham and Davis,[44] and Barnault et al.[45] show that vibrationally excited $I_2(X)$ is produced in $I_2/O_2(a)$ mixtures. Van Bentham and Davis[44] estimated that the $[I_2(X, v > 32)]/[I_2(X)]$ ratio was around 2.5×10^{-4} for a flow-tube experiment where $O_2(a)$ was generated using a microwave discharge. It is quite possible that energy-transfer events of the type $I_2(X, v \geq 10) + O_2(a) \rightarrow I_2(A', A) + O_2(X)$ contribute to the excitation of $I_2(A', A)$, as proposed by Barnault et al.[45] Inclusion of these channels in the revised kinetic model will be explored in a future study. This might improve the agreement between the observed and simulated data in the region where the dissociation is accelerating.

VI. Conclusions

Overall, the I_2 dissociation mechanism outlined here yields simulations that are in reasonably good agreement with our flow-tube experiments. The obvious weakness of the model is that, like the standard package, it still contains many assumed values for unmeasured rate constants and branching fractions. The excitation probabilities for O_2 and I_2 vibrational levels in the proposed E-V processes are unknown. The values of the rate constant of key reactions (95–97) are, at present, just fitting parameters.

In addition to probing the dissociation mechanism, the present experimental results also have a significant practical implication. It was found that the presence of a moderate pressure of CO_2 does not inhibit the I_2 dissociation process under the conditions of a typical COIL device. This is consistent with the findings of Ref. 34, in which it was demonstrated that CO_2 can be used effectively as an inexpensive carrier gas for COIL. This circumstance opens a new possibility for the development of both open- and closed-cycle COILs that utilize cryogenic pumps.

Acknowledgments

We gratefully acknowledge support of this work by the U.S. Civilian Research and Development Foundation through Grant

RC1-2516-SA-03 and the Air Force Office of Scientific Research through Multidisciplinary Research Initiative Grant AFOSR F49620-02-1-0357.

References

[1]Rybalkin, V., Katz, A., Barmashenko, B. D., and Rosenwaks, S., "Nearly Attaining the Theoretical Efficiency of Supersonic Chemical Oxygen–Iodine Laser," *Applied Physics Letters,* Vol. 85, No. 24, 2004, pp. 5851–5853.

[2]Perram, G. P., "Approximate Analytic Solution for the Dissociation of Molecular Iodine in the Presence of Singlet Oxygen," *International Journal of Chemical Kinetics*, Vol. 27, No. 8, 1995, pp. 817–828.

[3]Lawrence, W. G., Van Marter, T. A., Nowlin, M. L., and Heaven, M. C., "Inelastic Collision Dynamics of Vibrationally Excited $I_2(X)$," *Journal of Chemical Physics*, Vol. 106, No. 1, 1997, pp. 127–141.

[4]Lilenfeld, H. V., "Oxygen–Iodine Laser Kinetics," McDonnell Douglas Research Lab., Final Rept., AFWL-TR-83-1, St. Louis, MO, May 1983.

[5]Heaven, M. C., Komissarov, A. V., and Goncharov, V., "Mechanism and Kinetics of Iodine Dissociation in COIL," *Proceedings of SPIE*, Vol. 4631, May 2002, pp. 13–22.

[6]Han, J., Komissarov, A. V., Tinney, S. P., and Heaven, M. C., "Kinetic Studies for Advanced Iodine Laser Concepts," *Proceedings of SPIE*, Vol. 5777, March 2005, pp. 198–206.

[7]Derwent, R. G., and Thrush, B. A., "Excitation of Iodine by Singlet Molecular Oxygen 1," *Journal of the Chemical Society, Faraday Transactions 2: Molecular and Chemical Physics*, Vol. 68, 1972, pp. 720–728.

[8]Derwent, R. G., Kearns, D. R., and Thrush, B. A., "The Excitation of Iodine by Singlet Molecular Oxygen," *Chemical Physics Letters*, Vol. 6, No. 2, 1970, pp. 115–116.

[9]Aviles, R. G., Muller, D. F., and Houston, P. L., "Quenching of Laser-Excited $O_2(b^1\Sigma_g^+)$ by CO_2, H_2O and I_2," *Applied Physics Letters*, Vol. 37, No. 4, 1980, pp. 358–360.

[10]Muller, D. F., Young, R. H., and Houston, P. L., "Direct Observation of Diatomic Iodine Collisional Dissociation by $O_2(b)$," *Applied Physics Letters*, Vol. 38, No. 6, 1981, pp. 404–406.

[11]Heaven, M. C., Han, J., Davis, S. J., and Lee, S., "Re-Examination of the Role of $O_2(b)$ in the I_2 Dissociation Mechanism," *Proceedings of SPIE*, Vol. 5334, May 2004, pp. 53–59.

[12]Arnold, S. J., Finlayson, N., and Ogryzlo, E. A., "Some Novel Energy-Pooling Processes Involving $O_2(^1\Delta)$," *Journal of Chemical Physics*, Vol. 44, No. 6, 1966, pp. 2529–2531.

[13]Heidner, R. F., Gardner, C. E., Segal, G. I., and El-Sayed, T. M., "Chain-Reaction Mechanism for I_2 Dissociation in the $O_2(^1\Delta)$-I Atom Laser," *Journal of Physical Chemistry*, Vol. 87, No. 13, 1983, pp. 2348–2360.

[14]David, D., "Analysis of the A-X System of Iodine from Its Infrared Emission Spectrum," *Chemical Physics Letters*, Vol. 93, No. 1, 1982, pp. 16–20.

[15]Macler, M., Nicolai, J. P., and Heaven, M. C., "Electronic Spectroscopy and Energy Transfer Pathways of Matrix Isolated Iodine," *Journal of Chemical Physics*, Vol. 91, No. 2, 1989, pp. 674–682.

[16]Nota, M., Bouvier, A. J., Bacis, R., Bouvier, A., Crozet, P., Churassy, S., and Koffend, J. B., "The Dissociation of Iodine by Singlet Molecular Oxygen; Role of the Vibrational Reservoir State $A'(2u)$," *Journal of Chemical Physics*, Vol. 91, No. 3, 1989, pp. 1938–1940.

[17]Browne, R. J., and Ogryzlo, E. A., "Chemiluminescence from the Reaction of Cl_2 with Aqueous H_2O_2," *Proceedings of the Chemical Society*, Vol. 117, April 1964, pp. 89–91.

[18]Azyazov, V. N., Nikolaev, V. D., Svistun, M. I., and Ufimtsev, N. I., "Luminescence of the Oxygen Dimole at the Output of a Chemical Singlet-Oxygen Generator," *Quantum Electronics*, Vol. 29, No. 9, 1999, pp. 767–771.

[19]Antonov, I. O., Azyazov, V. N., and Ufimtsev, N. I., "Experimental and Theoretical Study of Distribution of O_2 Molecules over Vibrational Levels in $O_2(a^1\Delta_g)$-I Mixture," *Journal of Chemical Physics,* Vol. 119, No. 20, 2003, pp. 10,638–10,646.

[20]Komissarov, A. V., Goncharov, V., and Heaven, M. C., "Chemical Oxygen-Iodine Laser (COIL) Kinetics and Mechanisms," *Proceedings of SPIE*, Vol. 4184, Jan. 2001, pp. 7–12.

[21]Kalogerakis, K. S., Copeland, R. A., and Slanger, T. G., "Collisional Removal of $O_2(b, v=2,3)$," *Journal of Chemical Physics,* Vol. 116, No. 12, 2002, pp. 4877–4885.

[22]Tellinghuisen, J., and Phillips, L. F., "Kinetics of I_2 Following Photolysis at 1930 Å: Temperature Dependence of A′-State Quenching," *Journal of Physical Chemistry*, Vol. 90, No. 21, 1986, pp. 5108–5120.

[23]Parker, J. G., and Ritke, D. N., "Collisional Deactivation of Vibrationally Excited Singlet Molecular Oxygen," *Journal of Chemical Physics*, Vol. 59, No. 7, 1973, pp. 3713–3722.

[24]Britan, A. B., and Starik, A. M., "The Study of Vibrationally Nonequilibrium Flow in the CO_2-N_2-O_2-H_2O Mixture," *Zhurnal Prikladnoi Mekhaniki i Tekhnicheskoi Fiziki*, No. 4, 1980, pp. 41–50 (in Russian).

[25]Kalogerakis, K. S., Copeland, R. A., and Slanger, T. G., "Vibrational Energy Transfer in $O_2(X^3\Sigma, v=2, 3)+O_2$ Collisions at 330 K," *Journal of Chemical Physics*, Vol. 123, No. 4, 2005, 044309.

[26]Hwang, E. S., Copeland, R. A., and Slanger, T. G., "Collisional deactivation of $O_2(a^1\Delta_g, v=1,2)$," *Journal of Chemical Physics* (in preparation).

[27]Lopez-Puertas, M., Zaragoza, G., Kerridge, B. J., and Taylor, F. W., "Non-Local Thermodynamic Equilibrium Model for H_2O 6.3 and 2.7-μm Bands in the Middle Atmosphere," *Journal of Geophysical Research*, Vol. 100, No. D5, 1995, pp. 9131–1942.

[28]Finzi, J., Hovis, F. E., Panfilov, V. N., Hess, P., and Moore, C. B., "Vibrational Relaxation of Water Vapor," *Journal of Chemical Physics*, Vol. 67, No. 9, 1977, pp. 4053–4061.

[29]Biryukov, A. S., and Shcheglov, V. A., "Kinetics of Processes in an Iodine–Oxygen Laser," *Soviot Journal of Quantum Electronics*, Vol. 16, No. 3, 1986, pp. 333–337.

[30]Antonov, I. O., Azyazov, V. N., Pichugin, S. Yu., and Ufimtsev, N. I., "Detection of Vibrationally Excited O_2 in $O_2(a^1\Delta_g)$-I Mixture," *Chemical Physics Letters*, Vol. 376, No. 1–2, 2003, pp. 168–173.

[31]Paschkewitz, J., Shang, J., Miller, J., and Madden, T., "An Assessment of COIL Physical Property and Chemical Kinetic Modeling Methodologies," AIAA Paper 2000-2574, June 2000.

[32]Heidner, R. F., III, Gardner, C. E., El-Sayed, T. M., Segal, G. I., and Kasper, J. V. V., "Temperature Dependence of $I(^2P_{1/2})+O_2(^1\Delta)$ Energy Pooling," *Journal of Chemical Physics*, Vol. 74, No. 10, 1981, pp. 5618–5626.

[33]Newman, S. M., Lane, I. C., and Orr-Ewing, A. J., "Integrated Absorption Intensity and Einstein Coefficient for the $O_2a^1\Delta_g - X^3\Sigma_g^-$ (0,0) Transition: A Comparison of Cavity Ringdown High Resolution Fourier Transform Spectroscopy with a Long-Path Absorption Cell," *Journal of Chemical Physics*, Vol. 110, No. 22, 1999, pp. 10,749–10,757.

[34]Azyazov, V. N., Safonov, V. S., and Ufimtsev, N. I., "Efficient Subsonic Chemical Oxygen-Iodine Laser Operating Without Buffer Gas," *Proceedings of SPIE*, Vol. 4760, Sept. 2002, pp. 942–946.

[35]Khvatov, N. A., Nikolaev, V. D., Svistun, N. I., Zagidullin, M. V., and Hager, G. D., "Results of Small-Signal Gain Measurements on a Supersonic Chemical Oxygen-Iodine Laser with an Advanced Nozzle Bank," *IEEE Journal of Quantum Electronics*, Vol. 38, No. 5, 2002, pp. 421–428.

[36]Tellinghuisen, J., Whyte, A. R., and Phillips, L. F., "Kinetics of I_2 Following ArF Laser Excitation: Thermal Dissociation of the $A'(2_u)$ State," *Journal of Physical Chemistry*, Vol. 88, No. 25, 1984, pp. 6084–6087.

[37]Antonov, I. O., Azyazov, V. N., Pichugin, S. Yu., and Ufimtsev, N. I., "Role of Vibrationally Exited $O_2(^1\Delta)$ in COIL," *Proceedings of SPIE*, Vol. 5777, March 2005, pp. 78–86.

[38]Azyazov, V. N., Safonov, V. S., and Ufimtsev, N. I., "Dissociation of I_2 and the Vibrational Kinetics in the Oxygen-Iodine Medium," *Quantum Electronics*, Vol. 30, No. 8, 2000, pp. 687–693.

[39]Coletti, C., and Billing, G. D., "Vibrational Energy Transfer in Molecular Oxygen Collisions," *Chemical Physics Letters*, Vol. 356, No. 1–2, 2002, pp. 14–22.

[40]Gordiets, B. F., Osipov, A. I., and Shelepin, L. A., *Kinetic Processes in Gases and Molecular Lasers,* Nauka, Moscow, 1980, p. 127 (in Russian).

[41]Azyazov, V. N., Gorokhov, A. V., Pichugin, S. Yu., Safonov, V. S., and Ufimtsev, N. I., "Vibrational Energy Distribution of Oxygen in the Active Medium of COIL," *Proceedings of SPIE*, Vol. 4706, June 2002, pp. 18–23.

[42]Antonov, I. O., Azyazov, V. N., Pichugin, S. Y., and Ufimtsev, N. I., "Calculation of O_2 Molecules Distribution over Vibrational Levels in Chemical Oxygen-Iodine Laser," *Proceedings of SPIE*, Vol. 5479, June 2004, pp. 59–66.

[43]Hall, G. E., Marinelli, W. J., and Houston, P. L., "Electronic-to-Vibrational Energy Transfer from Excited Atomic Iodine ($I^*(5^2P_{1/2})$) to Molecular Iodine ($25 < v < 43$)," *Journal of Physical Chemistry,* Vol. 87, No. 12, 1983, pp. 2153–2161.

[44]Van Benthem, M. H., and Davis, S. J., "Detection of Vibrationally Excited I_2 in the Iodine Dissociation Region of Chemical Oxygen–Iodine Laser," *Journal of Physical Chemistry*, Vol. 90, No. 5, 1986, pp. 902–905.

[45]Barnault, B., Bouvier, A. J., Pigashe, D., and Bacis, R., "Absolute Measurements of the Molecular Iodine High Vibrational Levels in the Oxygen–Iodine Reaction," *Journal of Physics IV*, Vol. 1, No. 7, 1991, pp. C7/647–C7/650.

R. Lucht
Associate Editor